ESD-TR-74-366

MTR-2921

THE DEVELOPMENT OF SURFACE WAVE DISPERSIVE FILTERS FOR USE IN A MULTICHANNEL PULSE COMPRESSION SYSTEM

W. M. Bridge

FEBRUARY 1975

Prepared for

DEPUTY FOR PLANNING TECHNOLOGY AND REQUIREMENTS
ELECTRONIC SYSTEMS DIVISION
AIR FORCE SYSTEMS COMMAND
UNITED STATES AIR FORCE
Hanscom Air Force Base, Bedford, Massachusetts

Project No. 7060

Prepared by

THE MITRE CORPORATION
Bedford, Massachusetts
Contract No. F19628-73-C-0001

REVIEW AND APPROVAL

This technical report has been reviewed and is approved for publication.

John F Donegan

JOHN F. DONEGAN, GS-13
Project Engineer

FOR THE COMMANDER

Anthony P. Trunfio

ANTHONY P. TRUNFIO, Technical Director
Directorate of Technology
Deputy for Planning Technology
and Requirements

UNCLASSIFIED

SECURITY CLASSIFICATION OF THIS PAGE *(When Data Entered)*

REPORT DOCUMENTATION PAGE		READ INSTRUCTIONS BEFORE COMPLETING FORM
1. REPORT NUMBER ESD-TR-74-366	2. GOVT ACCESSION NO.	3. RECIPIENT'S CATALOG NUMBER
4. TITLE *(and Subtitle)* THE DEVELOPMENT OF SURFACE WAVE DISPERSIVE FILTERS FOR USE IN A MULTICHANNEL PULSE COMPRESSION SYSTEM		5. TYPE OF REPORT & PERIOD COVERED 6. PERFORMING ORG. REPORT NUMBER MTR-2921
7. AUTHOR(s) W.M. Bridge		8. CONTRACT OR GRANT NUMBER(s) F19628-73-C-0001
9. PERFORMING ORGANIZATION NAME AND ADDRESS The MITRE Corporation Box 208 Bedford, MA 01730		10. PROGRAM ELEMENT, PROJECT, TASK AREA & WORK UNIT NUMBERS Project No. 7060
11. CONTROLLING OFFICE NAME AND ADDRESS Deputy for Planning Technology and Requirements Electronic System Division, AFSC Hanscom Air Force Base, Bedford, MA 01731		12. REPORT DATE FEBRUARY 1975 13. NUMBER OF PAGES 62
14. MONITORING AGENCY NAME & ADDRESS*(if different from Controlling Office)*		15. SECURITY CLASS. *(of this report)* UNCLASSIFIED 15a. DECLASSIFICATION/DOWNGRADING SCHEDULE

16. DISTRIBUTION STATEMENT *(of this Report)*

Approved for public release; distribution unlimited.

17. DISTRIBUTION STATEMENT *(of the abstract entered in Block 20, if different from Report)*

18. SUPPLEMENTARY NOTES

19. KEY WORDS *(Continue on reverse side if necessary and identify by block number)*

DISPERSIVE FILTER
PULSE COMPRESSION
SURFACE WAVE

20. ABSTRACT *(Continue on reverse side if necessary and identify by block number)*

The technology and understanding of acoustic surface wave devices has progressed to the point where they can be used to implement sophisticated processing schemes such as a parallel channel pulse compression filter. This report discusses the design, development and experimental verification of the surface wave dispersive networks necessary to build a 7-channel pulse compression filter with 700 MHz bandwidth and a TW product of 4900. These individual channel filters must be time contiguous with identical linear FM dispersive characteristics. A division synthesis

DD FORM 1 JAN 73 1473 EDITION OF 1 NOV 65 IS OBSOLETE

UNCLASSIFIED

SECURITY CLASSIFICATION OF THIS PAGE *(When Data Entered)*

technique is developed for the realization of these filters. The technique is specifically tailored for an acoustic surface wave implementation consisting of one apodized and one unapodized transducer. The actual filter design and fabrication were carried out at Hughes. The resulting filters were quite reproducible and their general characteristics (spectrum shape, bandwidth, and dispersive delay) were essentially as desired.

TABLE OF CONTENTS

LIST OF ILLUSTRATIONS

SECTION

BACKGROUND

The primary object of Project 7060 (Microwave and Digital Signal Processing Techniques) has been to demonstrate the practical feasibility of a parallel channel dispersive filter utilizing surface wave components for the individual channel dispersive networks. The FY 73 effort included the development of a synthesis procedure for the realization of time-contiguous dispersive filters. As a result of this effort, a sub-contract was issued to Hughes Aircraft Company for the fabrication of seven such filters with the potential for realizing a parallel channel pulse compression system having 700 MHz bandwidth and a TW product of 4900.

The minimal effort for FY 74 (1/4 man-year), has been concerned with technical monitoring of the Hughes contract. This contract involved some cooperative effort between Hughes and MITRE for the development of acoustic devices based on the MITRE waveform synthesis procedure and the Hughes circuit model analysis of surface wave transducers. The cooperative effort was quite satisfactory and beneficial to both parties. Hughes received the benefit of the tested MITRE synthesis programs while MITRE retained the advantage of close contact

with the contractor. Three design iterations were carried out, with the actual device fabrication based on the final design. Although the acoustic device fabrication took longer than expected, the early test results as witnessed by a MITRE representative looked very promising. The MITRE division synthesis technique was essentially validated. The final device characteristics were quite repeatable and were well predicted by the Hughes transducer analysis program. Although time does not permit the actual implementation of a multi-channel dispersive filter, the acoustic devices have been delivered along with complete experimental frequency response data for each network. This frequency response data is on digital tape and the performance of the seven channel dispersive filter could be obtained from a computer analysis of this data. This would be a particularly interesting task to perform because it could demonstrate the feasibility of a complete seven channel filter with a TW product of 5000 without incurring the expense of a hardware implementation.

The remainder of the FY 74 effort has been devoted to the writing of this final report.

SECTION 2

DEVELOPMENT OF TIME-CONTIGUOUS SURFACE WAVE DISPERSIVE FILTERS

The MITRE synthesis procedure for the realization of time-contiguous dispersive filters has been presented previously. This is a procedure for realizing a linear FM impulse response with an envelope which tapers to zero at either end according to a prescribed cosine law. This taper results in a good approximation to a band-limited signal. In addition, the cosine function possesses odd symmetry about its midpoint so that adjacent channels can be added contiguously, as shown in Figure 1, without introducing a discontinuity in the combined impulse response. This diagram clearly indicates the critical nature of both the phase and time delay in the transition region if both signals are to add to a constant magnitude. In addition, the diagram points up the fact that the resulting overall dispersion (T) is N times the dispersion of a single channel (ΔT) and that the overall bandwidth (W) is N times the bandwidth of a single channel (ΔW) where N is the number of channels. Thus the TW product for an N channel filter is N^2 times the TW product of the individual channel dispersive networks.

$$TW = N^2 (\Delta T \, \Delta W) \tag{1}$$

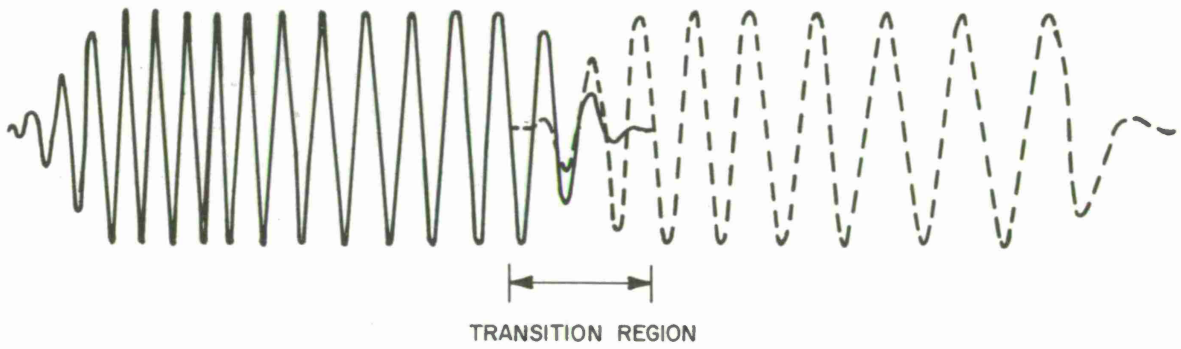

Figure 1 TIME-CONTIGUOUS DISPERSIVE FILTER CHARACTERISTICS

The TW product of a linear FM filter is a measure of the filter's effectiveness in a radar, communications, or spectral analysis application and Equation (1) shows the distinct advantages to be gained from a large number of channels. The complication of the overall filter, of course, increases with the number of channels so it behooves the designer to use as large a $\Delta T\ \Delta W$ product in the individual channel filters as is practical. Recent advances in acoustic surface wave technology have made it practical to consider individual channel bandwidths on the order of 100 MHz and $(\Delta T\ \Delta W)$ products of 100. Such devices are quite practical with current photo-lithography techniques and the parallel channel approach could yield filter bandwidths well in excess of the current capabilities for a single acoustic device.

The contract awarded to Hughes was for the development of seven individual channel dispersive filters each with a bandwidth (ΔW) of 100 MHz centered at 300 MHz and with dispersive delays (ΔT) of 1.0 μsec. In addition the fixed, non-dispersive delay of each successive filter was incremented by 1.0 μsec so that the resulting impulse responses could be added contiguously, after appropriate frequency translations. These seven acoustic dispersive filters have been fabricated and tested extensively at Hughes. This testing includes complete frequency response data, both amplitude and phase, for each of the seven acoustic networks. These data were taken with an automatic network analyzer and are recorded in digital form on magnetic tape. The

data was taken every 0.2 MHz from 198 MHz to 403 MHz and is more than sufficient to perform Fourier transform analysis.

SECTION 3

THEORETICAL CONSIDERATIONS

The MITRE synthesis procedure is specifically tailored for an acoustic surface wave implementation consisting of distinct input and output transducers separated by a non-dispersive delay medium. The desired linear FM waveform can be expressed in the time domain by:

$$h(t) = a(t)\, e^{j\phi(t)} \tag{2}$$

where $h(t)$ denotes the impulse response, $a(t)$ is the desired envelope function as indicated in Figure 1 and $\phi(t)$ is the quadratic phase function required for a linear FM signal. The spectrum or frequency response of such a time waveform can be obtained by taking the Fourier transform of this impulse response.

$$H(f) \Longleftrightarrow h(t)$$

The Fourier transform of the desired impulse response can be obtained most readily with the aid of a digital computer although closed form solutions involving Fresnel integrals have been obtained for the special case of an abrupt modulation envelope. The computed spectra

for various tapered linear FM impulse responses are shown in Figure 2. These results clearly indicate that envelope tapering reduces the "Fresnel ripples" and increasingly band-limits the signal.

The acoustic surface wave implementation of any filter function requires the use of two transducers (input and output) each of which exhibits its own frequency response. Thus the desired frequency response $H(f)$ must be synthesized as the product of two transducer frequency response functions.

$$H(f) = G_1(f) \cdot G_2(f) \tag{3}$$

In general, the individual transducer frequency response functions $G_1(f)$ and $G_2(f)$ are synthesized by tapering the finger overlap or apodization, which in effect varies the acoustic beamwidth as prescribed by the desired frequency response. However, for the separation implied by Equation (3) to be strictly valid, one transducer must remain unapodized with a uniform acoustic beamwidth W_o, while the second transducer must have a maximum acoustic beamwidth no greater than W_o.

$$W_{max} \leq W_o$$

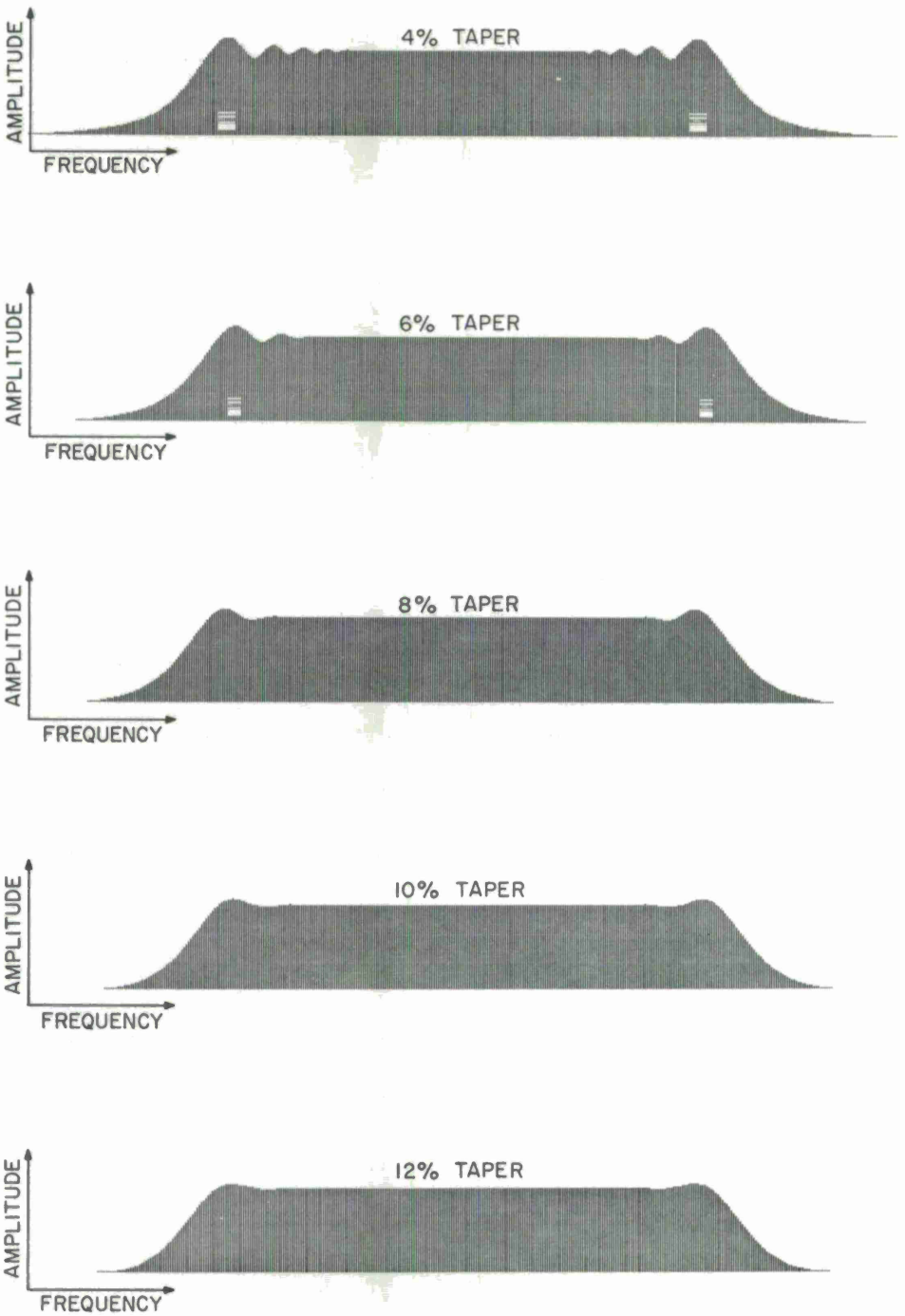

IA-40,465

Figure 2 SPECTRA FOR TAPERED LINEAR FM IMPULSE RESPONSES

Under these conditions the desired frequency response, $H(f)$, is separable and can be expressed as:

$$H(f) = \left\{ \sum_{n=1}^{N} I_o \, e^{j2\pi f \frac{X_n}{v}} \right\} \cdot \left\{ \sum_{m=1}^{M} I_m \, e^{-j2\pi f \frac{Y_m}{v}} \right\} \qquad (4)$$

where N is the total number of fingers in the unapodized transducer and M is the total number of fingers in the apodized transducer. I_o is a constant related to the uniform apodization of transducer #1 while I_m is related to the variable apodization of transducer #2. X_n and Y_m represent the electrode or finger positions of the unapodized and apodized transducers. The factor v is the acoustic surface wave velocity. Equation (4) implies that the two transducers can be synthesized independently except for the constraint that transducer #1 must be unapodized.

Before continuing with this specific synthesis technique, it is worth reviewing the general tapped delay line synthesis of band-limited signals in the frequency domain. Shannon's Sampling Theorem states that if the Fourier transform of a given time function $f(t)$ is zero above a certain frequency ω_c then $f(t)$ can be uniquely defined from its values sampled as times $\frac{n\pi}{\omega_c}$.[1]

Thus

$$f(t) = \sum_{n=-\infty}^{\infty} f_n \frac{\sin(\omega_c t - n\pi)}{(\omega_c t - n\pi)} \tag{5}$$

where $f_n = f\left(\frac{n\pi}{\omega_c}\right)$.

Because of the infinite summation, the time function for a band-limited signal is infinite in extent, and it becomes an approximation problem to establish how few samples are required to adequately represent the function.

The situation for an acoustic surface wave device is somewhat different, for here the sample times are well defined by the location of the transducer fingers and the total length of the time function is limited by the combined length of the two transducers. Thus the surface wave implementation implies time-limited signals which inherently have infinite bandwidth and cannot be sampled at a finite rate. On the other hand, it was shown in Figure 2 that the cosine tapered linear FM impulse response was effectively band-limited at a frequency somewhat higher than the reciprocal of the highest period in the impulse response. For example, with a 7% taper and 1 μsec of dispersion over 250 MHz to 350 MHz, the spectrum was down only 6 dB at the 250 MHz and 350 MHz points but down 30 dB at 236 MHz and 364 MHz. From this, one might assume that samples taken uniformly every 1.375 Ns would provide an adequate representation of the signal.

In the usual tapped delay synthesis, each tap is provided with the appropriate amplitude and phase weighting necessary to realize the desired function. Unfortunately phase weighting is not possible for high frequency interdigital transducers where the individual finger-widths and spacings are on the order of microns. The amplitude weighting can, of course, be achieved by apodizing one transducer as mentioned previously. Thus the surface wave implementation requires that the taps be located where the desired impulse response function,

$$h(t) = a(t)\, e^{j\phi(t)} \quad ,$$

is real. If $\phi(t)$ is the quadratic phase function of a linear FM impulse response, then the taps (fingers) will be located where

$$\phi(t) = n\pi = \left(\omega_o\, t + \frac{\Delta T}{\Delta \omega} \, \frac{t^2}{2} \right) \quad .$$

This will, of course, result in non-uniform sampling and the question that comes to mind is: does this non-uniform sampling adequately represent the desired impulse response? Smith et al[2] have calculated the Fourier transform of an arbitrary impulse response,

$$g(t) = a(t)\, e^{j\phi(t)} \quad ,$$

with the following result:

$$G_s(f) \approx \frac{1}{\pi} \sum_{n=1}^{N} \frac{(-1)^n \, a(t_n)}{f_n} \sin\left(\frac{\pi}{2} \frac{f}{f_n}\right) e^{-j2\pi f t_n} \qquad (6)$$

$G_s(f)$ represents the spectrum of the real sampled impulse response, and t_n, the temporal position of the n^{th} electrode, is defined from the relationship:

$$\phi(t_n) = n\pi \quad .$$

The term f_n represents the synchronous frequency for which the n^{th} electrode spacing corresponds to $\lambda/2$. In order to resolve the question of adequate sampling, one would have to compare the spectrum $G_s(f)$ of the non-uniformly sampled signal with the spectrum of the continuous function. This direct comparison has not been made but the Hughes transducer analysis program, which is very nearly equivalent, indicated that the mid-band ripple in the spectrum introduced by this required non-uniform sampling is on the order of $\pm$ 1/2 dB.

The Hughes transducer analysis program is based on the Mason cross-field equivalent circuit of an interdigital transducer, shown in Figures 3 and 4. It was shown by H. M. Gerard[3] that the acoustic stress generated at port 1 or 2 for the n^{th} transducer finger can be expressed as:

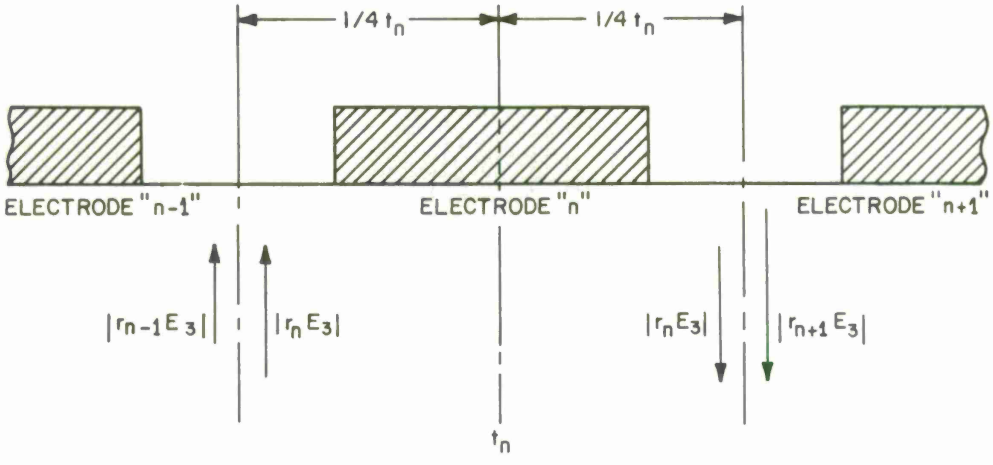

Figure 3 δ- FUNCTION STRESS SOURCES CORRESPONDING TO APPLIED ELECTRICAL VOLTAGE IMPULSE

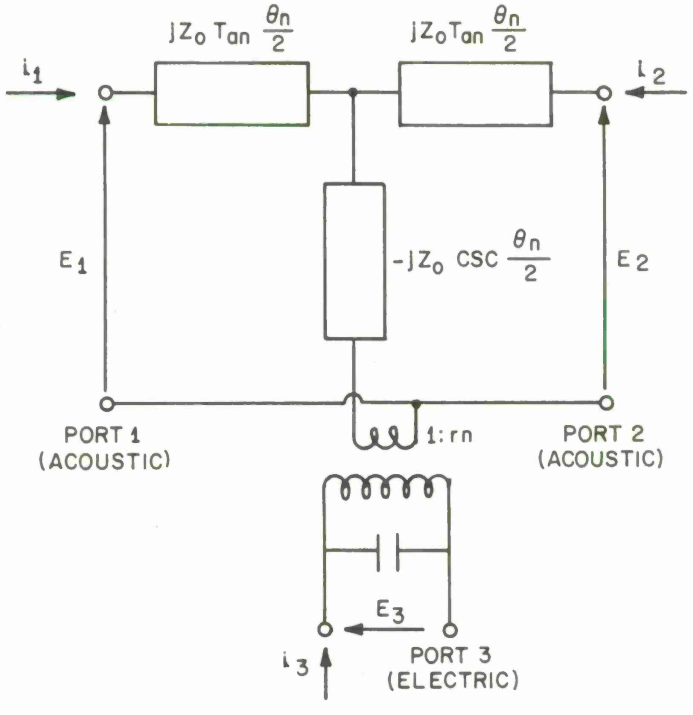

Figure 4 EQUIVALENT CIRCUIT FOR THE CROSSED FIELD MODEL OF A SINGLE ELECTRODE SECTION (MASON MODEL)

$$E_{1n}(f) = -e^{j\frac{\theta_n}{2}} \left[j\, r_n \sin \frac{\theta_n}{2} \right] E_3 \qquad (7)$$

where r_n is the electric to acoustic turns ratio and E_3 is the electric voltage applied to port 3. The term θ_n is the acoustic length of the n^{th} section:

$$\theta_n = 2\pi \frac{L_n}{\lambda} \quad \text{or} \quad \frac{2\pi f}{V} L_n$$

where λ is the acoustic wavelength and L_n is the average center-to-center spacing between the n^{th} electrode and its nearest neighbors. By referencing the acoustic stress to the middle of the n^{th} electrode, then Equation (7) can be simplified to:

$$E_{1n} = j r_n \sin \frac{\theta_n}{2} E_3 \,. \qquad (8)$$

The Fourier transform of Equation (8) is given below and demonstrates that the impulse response of a single electrode is equivalent to a pair of acoustic δ-function stress sources located one quarter period on either side of the electrode center.

$$E_{1n}(t) = -\frac{1}{2} r_n E_3 \left[\delta\left(t - \frac{t_n}{4}\right) - \delta\left(t + \frac{t_n}{4}\right) \right] \qquad (9)$$

The equivalent circuit of Figure 4 was chosen because it readily allows for the cascading of sections in a multi-electrode transducer. If the transducer is driven from a zero impedance voltage source, then the total acoustic stress is the sum of the stresses generated by each finger, shifted by the appropriate phase length t_n to get to the acoustic output port of the entire transducer. Thus the total acoustic stress at the output port can be represented as follows:

$$E_1(f) = j\left[\sum_{n=1}^{N} r_n \sin\left(\frac{\pi}{2}\ \frac{f}{f_n}\right) e^{-j2\pi f\ t_n}\right] E_3 \qquad (10)$$

The electric-to-acoustic transfer function $T_{13}(f)$ is defined such that its magnitude squared, $|T_{13}(f)|^2$, represents the ratio of the power delivered to an acoustic beam divided by the maximum available power from the generator.

$$|T_{13}(f)|^2 \equiv \frac{\left|\frac{E_1}{E_3}\right|^2 \frac{1}{Z_o}}{\left|\frac{E_g}{E_3}\right|^2 \frac{1}{4R_g}} \qquad (11)$$

$$T_{13}(f) = 2\sqrt{\frac{R_g}{Z_o}}\ \frac{\frac{E_1}{E_3}}{\frac{E_g}{E_3}} = \frac{2}{\sqrt{Z_o G_g}}\ \frac{\frac{E_1}{E_3}}{\frac{E_g}{E_3}} \qquad (12)$$

The factor E_1/E_3 has already been defined by Equation (10) where

$$r_n = (-1)^n \sqrt{2 f_n C_n k^2 Z_o} \quad .$$

With a real generator of finite internal resistance, the voltage appearing across the electrical terminals of the transducer E_3 is not the same as the generator voltage E_g and must be evaluated from the electrical input impedance of the transducer. Smith[4] has recently shown that the crossed-field circuit model is the best representation of actual surface wave devices built on Quartz and Lithium Niobate. The shunt electrical equivalent circuit shown in Figure 5 is most suitable for this cross-field model. $Y_{rad}(f)$ is the acoustic radiation admittance and consists of both a real term, $G_a(f)$, and an imaginary term, $B_a(f)$. The energy dissipated in $G_a(f)$ is really the energy coupled into the acoustic beam by virtue of the piezo-electric coupling coefficient k. Because of the causality of the system, the imaginary term $B_a(f)$ is related to $G_a(f)$ by the Hilbert transform. In most situations, particularly

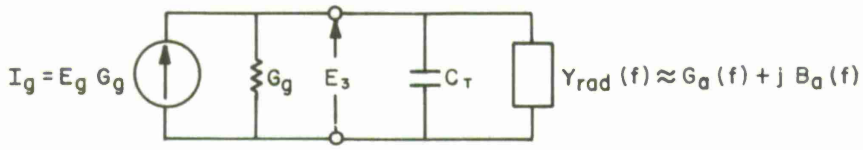

Figure 5 TRANSDUCER SHUNT EQUIVALENT CIRCUIRT

with low coupling materials such as Quartz, the magnitude of $y_{rad}(f)$ is much less than the susceptance of C_T. The ratio of the input terminal voltage E_3 to the generator voltage E_g can easily be calculated using the Norton equivalent current source.

$$\frac{E_3}{E_g} = \frac{1}{1 + \frac{j\omega C_T}{G_g} + \frac{Y_{rad}(f)}{G_g}} \qquad (13)$$

By choosing a convenient reference frequency, f_o, the above equation can be expressed in terms of dimensionless parameters Q_L and Q_r. Thus:

$$\frac{E_3}{E_g} = \frac{1}{1 + j\, Q_L \left(\frac{f}{f_o}\right) + \frac{Q_L}{Q_r}\, y_{rad}(f)} \tag{14}$$

where

$$Q_L \equiv \frac{2\pi f_o C_T}{G_g}\,, \quad Q_r \equiv \frac{2\pi f_o C_T}{G_a(f_o)}\,, \quad y_{rad}(f) \equiv \frac{Y_{rad}(f)}{G_a(f_o)}\,.$$

Using Equations (10), (12), and (14), the electric-to-acoustic transfer function can now be expressed as follows:

$$T_{13}(f) = \frac{2}{\sqrt{Z_o\, G_g}} \frac{j\left[\sum_{n=1}^{N} r_n \sin\left(\frac{\pi}{2}\,\frac{f}{f_n}\right) e^{-j2\pi f\, t_n}\right]}{1 + j\, Q_L\left(\frac{f}{f_o}\right) + \frac{Q_L}{Q_r}\, y_{rad}(f)} \tag{15}$$

The power transfer function $|T_{13}(f)|^2$ can now be expressed as follows:

$$|T_{13}(f)|^2 = \frac{8k^2}{G_g} \left| \frac{\sum_{n=1}^{N} (-1)^n \sqrt{f_n C_n} \sin\left(\frac{\pi}{2} \frac{f}{f_n}\right) e^{-j2\pi f t_n}}{1 + j\, Q_L \left(\frac{f}{f_o}\right) + \frac{Q_L}{Q_r}\, y_{rad}(f)} \right|^2 \qquad (16)$$

where $r_n = (-1)^n \sqrt{2 f_n C_n k^2 Z_o}$ was substituted into the above expression.

From the pure electrical circuit of Figure 5, $|T_{13}|^2$ can be viewed as the ratio of the power delivered to the load conductance $G_a(f)$ divided by the maximum available power from the generator. It must be remembered that only half the power delivered to $G_a(f)$ ends up in the desired acoustic wave. The remainder is converted into an acoustic wave propagating in the opposite direction which is intentionally absorbed. Thus the power transfer ratio to the desired acoustic wave is:

$$\left|T_{13}(f)\right|^2 = \frac{1}{2} \left|\frac{E_3}{E_g}\right|^2 \frac{G_a(f)}{G_g/4} = \frac{2}{G_g} \left|\frac{E_3}{E_g}\right|^2 G_a(f) \qquad (17)$$

Taking E_3/E_g from Equation (14) yields:

$$|T_{13}(f)|^2 = \frac{2}{G_g} \frac{G_a(f)}{\left|1 + j\, Q_L \left(\frac{f}{f_o}\right) + \frac{Q_L}{Q_r}\, y_{rad}(f)\right|^2} \tag{18}$$

Equations (18) and (16) are equivalent only if

$$G_a(f) = 4k^2 \left| \sum_{n=1}^{N} (-1)^n \sqrt{f_n C_n}\, \sin\left(\frac{\pi}{2}\, \frac{f}{f_n}\right) e^{-j2\pi f t_n} \right|^2 \tag{19}$$

We know from reciprocity that $T_{13}(f) = T_{31}(f)$. However, when analyzing an apodized transducer, it is convenient to consider it as an acoustic receiver illuminated by an acoustic beam of constant width W_o. It was stated previously that W_o must be equal to or greater than the maximum apodization of the receive transducer. If W_o is greater than W_{max} of the apodized transducer, some of the transmit energy by-passes the receive transducer and is lost. This does not change the shape of the transfer function $T_{31}(f)$. Thus without loss in generality W_1, the transmitter apodization can be assumed equal to the maximum apodization of the receiver (W_{max}) even if the

physical aperture of the transmitter is greater than W_{max}. Surface wave devices can have acoustic apertures on the order of 100 λ which implies that acoustic near field operation would have to be within $\frac{2d^2}{\lambda}$ or about 20,000 λ. Within this near field region, the surface acoustic power is considered uniform along a wavefront perpendicular to the direction of propagation. Thus the power received by the n^{th} finger of an apodized receive transducer is simply W_n/W_o times the incident power. Thus $T_{31}(f)$ for the apodized receive transducer can be obtained from Equation (15) with the following result.

$$T_{31}(f) = j2\sqrt{\frac{2k^2 W_o C_o}{G_g}} \left[\frac{\sum_{n=1}^{N} (-1)^h \sqrt{f_n} \left(\frac{W_n}{W_o}\right) \sin\left(\frac{\pi}{2} \frac{f}{f_o}\right) e^{-j2\pi f t_n}}{1 + j\, Q_L \left(\frac{f}{f_o}\right) + \frac{Q_L}{Q_r}\, y_{rad}(f)} \right] \tag{20}$$

where the substitution $C_n = W_n C_o$ has been included. The numerator of the second term is very similar to Equation (6), the spectrum for the real sampled representation of the desired impulse response. In fact if the aperture apodization is chosen so that

$$\sqrt{f_n} \left(\frac{W_n}{W_o}\right) = \frac{a(t_n)}{f_n} \tag{21}$$

then the numerator is within a constant, $1/\pi$, of the sampled impulse response. Equation (21) leads to the aperture weighting

law:

$$\frac{W_n}{W_o} = a(t_n)\,(f_n)^{-3/2} \tag{22}$$

Equation (20) states that if the apertures are chosen according to Equation (22), then the transfer function, $T_{13}(f)$ of this apodized transducer (when illuminated by a constant acoustic beamwidth, W_o) will be proportional to the Fourier transform of the real sampled version of the desired impulse response. This transfer function is also modified by the circuit factor

$$\left(1 + jQ_L \frac{f}{f_o}\right)$$

where the factor

$$\frac{Q_L}{Q_r}\, y_{rad}(f)$$

has been dropped because it is usually negligible. Equation (20) is basically an analysis expression for determining the transfer function spectrum of a given interdigital transducer.

The synthesis or waveform design problem is somewhat more complex for now the effect of the circuit factor must be included in the transducer design (apodization and finger positions) so that the ensuing transfer function is the desired Fourier transform of the real sampled impulse response. In order to solve the synthesis

problem a new function

$$\tilde{T}_{13}(f) \equiv T_{13}(f)\left[1 + j\, Q_L \frac{f}{f_o}\right]$$

is defined which is the Fourier transform of some new $\tilde{h}(t)$.

Thus

$$\tilde{T}_{13}(f) = \left[T_{13}(f) + j\, T_{13}(f) \frac{Q_L}{2\pi f_o}\, \omega\right] \tag{23}$$

and

$$\tilde{T}_{13}(f) \Longleftrightarrow \tilde{h}(t) = h(t) + \frac{Q_L}{2\pi f_o}\, \dot{h}(t) \tag{24}$$

where $\dot{h}(t)$ is the time derivative of the desired impulse response,

$$\dot{h}(t) = \frac{d}{dt}\left[a(t)\, e^{j\phi(t)}\right],$$

and is represented as follows:

$$\dot{h}(t) = j\, a(t)\, e^{j\phi(t)}\, \dot{\phi}(t) + e^{j\phi(t)}\, \dot{a}(t) \tag{25}$$

The transform of the new frequency response is

$$\tilde{h}(t) = \tilde{a}(t)\, e^{j\tilde{\phi}(t)}$$

where Smith et al (Reference 2) have shown that:

$$\left|\tilde{a}(t)\right|^2 = \left[a(t) + \frac{Q_L}{2\pi f_o}\,\dot{a}(t)\right]^2 + \left[\frac{Q_L}{2\pi f_o}\; a(t)\; e^{j\phi(t)}\right]^2 \tag{26}$$

$$\tilde{\phi}(t) = \phi(t) + \tan^{-1}\frac{Q_L\, a(t)\,\dot{\phi}(t)}{2\pi f_o\, a(t) + Q_L\,\dot{a}(t)} \tag{27}$$

Thus both the electrode positions and the apertures will have to be modified to account for the circuit factor introduced by the finite generator impedance. In addition the concept of synchronous frequency $\tilde{f}_n$ must be redefined as:

$$\tilde{f}_n = \frac{1}{2\pi}\,\frac{d}{dt}\,\tilde{\phi}(t) \tag{28}$$

It should be noted that the last three functions denoted by the $\sim$ symbol reduce to the previous definitions if the circuit effects are negligible (Q_L small). The new electrode positions and apertures can be obtained from the $\sim$ denoted functions just as before. Thus:

$$\tilde{\phi}(t_n) = n\pi \tag{29}$$

$$\frac{W_n}{W_o} \approx \tilde{a}(t) \cdot (\tilde{f}_n)^{-3/2} \qquad (30)$$

The development thus far has been based on the parallel equivalent circuit, which is most suitable for the Mason cross-field model. A series equivalent circuit shown in Figure 6 is also possible and may be more practical for low coupling materials such as Quarts where the capacitive susceptance $j\omega C_T$ greatly exceeds the radiation conductance $G_a(f)$.

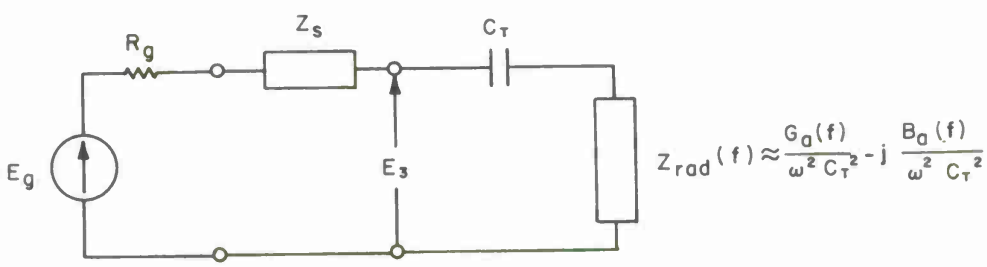

Figure 6 TRANSDUCER SERIES EQUIVALENT CIRCUIT

The primary difference is that the radiation resistance $R_a(f)$ now has a reciprocal ω^2 frequency term in addition to the normal frequency relationship of $G_a(f)$. Provision for a series tuning element which may be both inductive and resistive has also been included and a dual analysis can be carried out for this circuit. It can readily be shown if the capacitive reactance of C_T is much greater than $Z_{rad}(f)$ that:

$$\frac{E_3}{E_g} \approx \frac{-\,j\,Q_L\left(\frac{f_o}{f}\right)}{1 + j\,Q_L\left(\frac{f}{f_o} - \frac{f_o}{f}\right)} \tag{31}$$

where

$$Q_L \equiv \frac{1}{2\pi f_o (R_g + R_s)\, C_T}$$

and

$$f_o \equiv \frac{1}{2\pi} \frac{1}{\sqrt{L_s\, C_T}}$$

The power transfer function, $|T_{13}(f)|^2$, can now be expressed as follows using Equations (10), (12) and (31).

$$|T_{13}(f)|^2 = 8k^2 R_g \left| \frac{Q_L \left(\frac{f_o}{f}\right)}{1 + j Q_L \left(\frac{f}{f_o} - \frac{f_o}{f}\right)} \right|^2$$

$$\times \left| \sum_{n=1}^{N} (-1)^n \sqrt{f_n C_n} \sin\left(\frac{\pi}{2} \frac{f}{f_o}\right) e^{-j2\pi f t_n} \right|^2 \qquad (32)$$

The power transfer ratio for the electrical circuit of Figure 6 can also be represented as:

$$|T_{13}(f)|^2 = \frac{1}{2} \frac{I^2 \frac{G_a(f)}{\omega^2 C_T^2}}{\frac{E_g^2}{4R_g}} = \frac{1}{2} 4R_g \left| \frac{Q_L \left(\frac{f_o}{f}\right)}{1 + j Q_L \left(\frac{f}{f_o} - \frac{f_o}{f}\right)} \right|^2 G_a(f) \qquad (33)$$

Thus $G_a(f)$ is again represented by Equation (19) and the procedure for obtaining the apodized transfer function, $T_{13}(f)$, is very similar with the following result.

$$T_{13}(f) = 2\sqrt{2k^2\, C_o W_o R_g}\left[\frac{Q_L\left(\frac{f_o}{f}\right)}{1 + j\, Q_L\left(\frac{f}{f_o} - \frac{f_o}{f}\right)}\right] \tag{34}$$

$$\times \sum_{n=1}^{N} (-1)^n \sqrt{f_n}\left(\frac{W_n}{W_o}\right) \sin\left(\frac{\pi}{2}\,\frac{f}{f_n}\right) e^{-j2\pi f t_n}$$

where the substitution $C_n = W_n C_o$ has been included. The synthesis or waveform design problem is also similar with the exception that the required circuit factor is different.

$$\tilde{T}_{13}(f) = T_{13}(f)\left[\frac{1 + j\, Q_L\left(\frac{f}{f_o} - \frac{f_o}{f}\right)}{Q_L\left(\frac{f_o}{f}\right)}\right] \tag{35}$$

The new factor $\tilde{h}(t)$ is somewhat more complicated involving the $\int h(t)\, dt$ as well as $\dot{h}(t)$ but the procedure is similar and readily evaluated with the aid of a computer. It should be noted that Equation (35) does not reduce to $T_{13}(f)$ for a zero impedance voltage source $(R_g + R_s) = 0$ or $Q_L = \infty$. This is not surprising because the circuit

of Figure 6 includes a series tuning inductor L_s, and one would not expect the tuned frequency relationship to be the same as the untuned case. In the practical situation there is usually appreciable series resistance due to the thin metalization of the transducer fingers which is required to minimize local acoustic reflections at each finger edge. Thus in most situations the minimum series resistance is considerably larger than $R_a(f)$ and even with an ideal voltage source, the circuit Q would be relatively small.

In summary then, a procedure has been developed for the synthesis of a real sampled impulse response which includes the effects of circuit tuning elements and the effect of finite generator and load resistance. The synthesis procedure is based on the Mason crossed-field transducer model which was shown by Smith (Reference 4) to be most representative of Quartz and Lithium Niobate devices. The Hughes transducer analysis program is based on this model but can be used for either the series or parallel equivalent circuit and includes the effects of tuning elements. This program is basically a numerical evaluation of $T_{13}(f)$ from expressions like Equation (20) and (34), with input data coming directly from the geometry of the given transducers and the physical constants of the materials. The program is extremely versatile with the capability of handling most transducer analysis and design problems.

SECTION 4

DISPERSIVE FILTER SYNTHESIS

The details of this filter synthesis follow logically from the theoretical considerations. The MITRE waveform synthesis procedure was reported previously. This was basically a division synthesis procedure for the realization of a linear FM impulse response with an envelope which tapers to zero at either end according to a prescribed cosine law. The procedure resulted in the definition of two finite impulse response functions $h_1(t)$ and $h_2(t)$ whose convolution provided an excellent approximation of the desired impulse response. The first impulse response function $h_1(t)$ was constrained to have essentially constant magnitude while the remaining function $h_2(t)$ included any required variation in magnitude. Thus the waveform synthesis was tailored for a surface wave implementation consisting of one apodized and one unapodized transducer. This allows the desired frequency response, $H(f)$ to be synthesized as the product of the individual transducer frequency responses. Thus $H(f) = T_{13}(f) \times T_{31}(f)$ where $T_{13}(f)$ is the transfer function of the unapodized transducer and $T_{31}(f)$ is the transfer function of the apodized trandsucer. The frequency response of each series tuned transducer

consists of an array factor, a circuit factor and a scaling factor. For the series equivalent circuit, these factors can be obtained directly from Equation (34) with the following result

$$T_{13}(f) \text{ or } T_{31}(f) = 2\pi\sqrt{2k^2 C_o W_o R_g}\left[\frac{Q_L \frac{f_o}{f}}{1 + jQ_L\left(\frac{f}{f_o} - \frac{f_o}{f}\right)}\right] \cdot \left[G_s(f)\right] \qquad (36)$$

The factor $G_s(f)$, given by Equation (6) with

$$a(t_n) = \frac{W_n}{W_o}(f_n)^{3/2}$$

is simply the spectrum of the actual transducer with real samples. The middle term is the circuit factor for a series tuned transducer, where

$$Q_L \equiv \frac{1}{2\pi f_o (R_g + R_s) C_T} \quad .$$

The scaling factor at the beginning is a constant related to the geometry of the transducer and the Piezo-electric coupling coefficient of the material.

In general the design problem is to determine the necessary array factors $G_s(f)_{13}$ and $G_s(f)_{31}$ which establish the finger positions and apodization required to achieve the desired product

function, H(f). The array factor of the first transducer, $G_s(f)_{13}$, is known because transducer #1 was constrained to be unapodized with fingers located according to the classical linear FM impulse response. Thus $G_s(f)_{13}$ can be calculated directly from Equation (6) or the last term of Equation (34). The circuit and scaling factors for this transducer are also completely specified by its known geometry and the generator resistance. The static capacitance C_T and hence Q_L of this transducer is readily obtained from the known aperture width W_o. Thus $T_{13}(f)$ is completely specified from the known geometry and finger positions of the unapodized transducer.

The apodization and finger positions of the second transducer are, of course, unknown and must be determined. Although the total capacitance of the second transducer cannot be known exactly until its N apertures are specified, a good estimate can be obtained from the general shape of this transducer and the constraint that its maximum aperture must not exceed the uniform aperture of transducer #1. Sufficient information is now available to calculate an approximate value of $G_s(f)_{31}$ from the following expression:

$$H(f) = T_{13}(f) \cdot T_{31}(f) = T_{13}(f) \cdot K_{31}\, C_{31}(f)\, G(f)_{31}$$

where H(f) is the Fourier transform of the desired impulse response. K_{31} and $C_{31}(f)$ represent the known scaling factor and estimated

circuit factor for the apodized transducer. The factor $G(f)_{31}$ is the array factor (Fourier transform) of a continuous impulse response which will later be sampled at its real values to determine $G_s(f)_{31}$. The desired array factor $G(f)_{31}$ is obtained by dividing the product function $T_{13}(f) \cdot K_{31}\, C_{31}(f)$ into the desired frequency spectrum H(f). The finger position and aperture of transducer #2 can now be obtained from the inverse Fourier transform of $G(f)_{31}$. This time function, $g(t)_{31}$, is complex having both a real and imaginary part. The fingers are located where the function $g(t)_{31}$ is real (imaginary part is zero) and the acoustic aperture is determined by the magnitude of the function at each zero crossing of the imaginary part. In practice the function $g(t)_{31}$ is computed with a discrete Fourier transform routine which only has values at equally spaced intervals equal to the reciprocal of the sampling frequency. Thus, in order to accurately determine the magnitude of the function at each zero crossing, a cosine function was locally fitted to each cycle of data. The magnitude, $a(t_n)$, and zero crossings were then determined from the locally fitted cosine function, and the actual apertures were determined from the aperture weighting law, Equation (22). This completes the process of determining the apertures and finger positions for the apodized transducer. Now an exact value of static capacitance can be readily obtained. If this exact value of C_T is slightly greater than the estimated value one can simply scale down the overlap of each finger in the second transducer until the total capacity is

equal to the design value. This of course introduces some loss because a portion of the transmit beam bypasses the receive transducer. One could iterate this design procedure until this lost energy is minimized but on the Hughes design, it was less than 0.6 dB and for expediency, the iterative process was not performed.

This completes the design procedure and both transducers are completely defined. The Hughes transducer analysis program was then used to calculate the spectrum and impulse response of the entire device. This program calculates each transfer function from the physical constants of the material and the geometry of each transducer. The calculation actually evaluates Equation (34) at each desired frequency for all values of N. The overall frequency response is then obtained by taking the product of $T_{13}(f)$ and $T_{31}(f)$. The overall spectra and impulse response obtained from this circuit analysis program were very similar to the desired responses but a slight non-uniform ripple on the order of $\pm$ 1/2 dB was introduced into the functions. This ripple is attributed to the non-uniform sampling inherent in a linear FM transducer with real weighting coefficients as discussed previously.

The design procedure can be summarized with the following steps.

1. Design the unapodized transducer in the classical fashion to provide about half the total desired dispersion.

2. Include minimal apodization at the ends of this transducer to minimize ripples. (Apodized tails less than 3.3% of the dispersive time delay of the "unapodized" transducer.)

3. Calculate the transfer function, $T_{13}(f)$, for the "unapodized" transducer with the Hughes analysis program.

4. Calculate the scaling factor, K_{31}, and estimate the circuit factor $C_{31}(f)$ for the apodized transducer.

5. Calculate the array factor, $G(f)_{31}$, for the apodized transducer by dividing the product function $K_{31} \cdot C_{31}(f) \cdot T_{13}(f)$ into the desired impulse responses $H(f)$.

6. Calculate the discrete Fourier transform $g(t)_{31}$ of $G(f)_{31}$.

7. Locally fit a one cycle cosine function to the discrete data points of $g(t)_{31}$ to obtain accurate amplitude and zero crossing information.

8. Determine the apertures of the second transducer from the aperture weighting law and locate the fingers at points where the cosine fitted function is real.

9. Calculate the exact capacitance of the second transducer and scale down all the apertures of this transducer until the exact capacitance is equal to the estimated capacitance. Then, iterate the design process until the energy lost as a result of this aperture scaling is negligible.

10. Calculate the second transducer transfer function $T_{31}(f)$ from the Hughes transducer analysis program.

11. Multiply $T_{13}(f)$ by $T_{31}(f)$ to obtain the spectrum of the entire filter and inverse Fourier transform to obtain the impulse response of the entire filter.

12. Compare the computed spectrum and impulse response with the desired responses to determine if the design is adequate.

SECTION 5

RESULTS (THEORETICAL AND EXPERIMENTAL)

The feasibility of the division synthesis technique for the design of time-contiguous dispersive filters has been presented previously. This synthesis procedure was specifically tailored for an acoustic surface wave implementation consisting of one apodized and one unapodized transducer. The results of this waveform synthesis procedure are shown in Figure 7. This figure demonstrates that the time-contiguous linear FM signal can be synthesized approximately from the convolution of two time limited impulse responses, one of which has essentially uniform magnitude. This synthesis procedure formed the basis for the Hughes surface wave filter design.

The final Hughes filter design is shown in Figure 8 where the individual transducer apodizations were reproduced photographically from the actual 10X photo-masks. The upper frequency response function represents the product of the "unapodized" transfer function, $T_{13}(f)$, multiplied by the circuit and scaling factors of the apodized transducer. The second frequency response function represents the array factor for the time-limited impulse response which was used to obtain the apodization for transducer #2. The third frequency response function is the product of the previous two and represents the

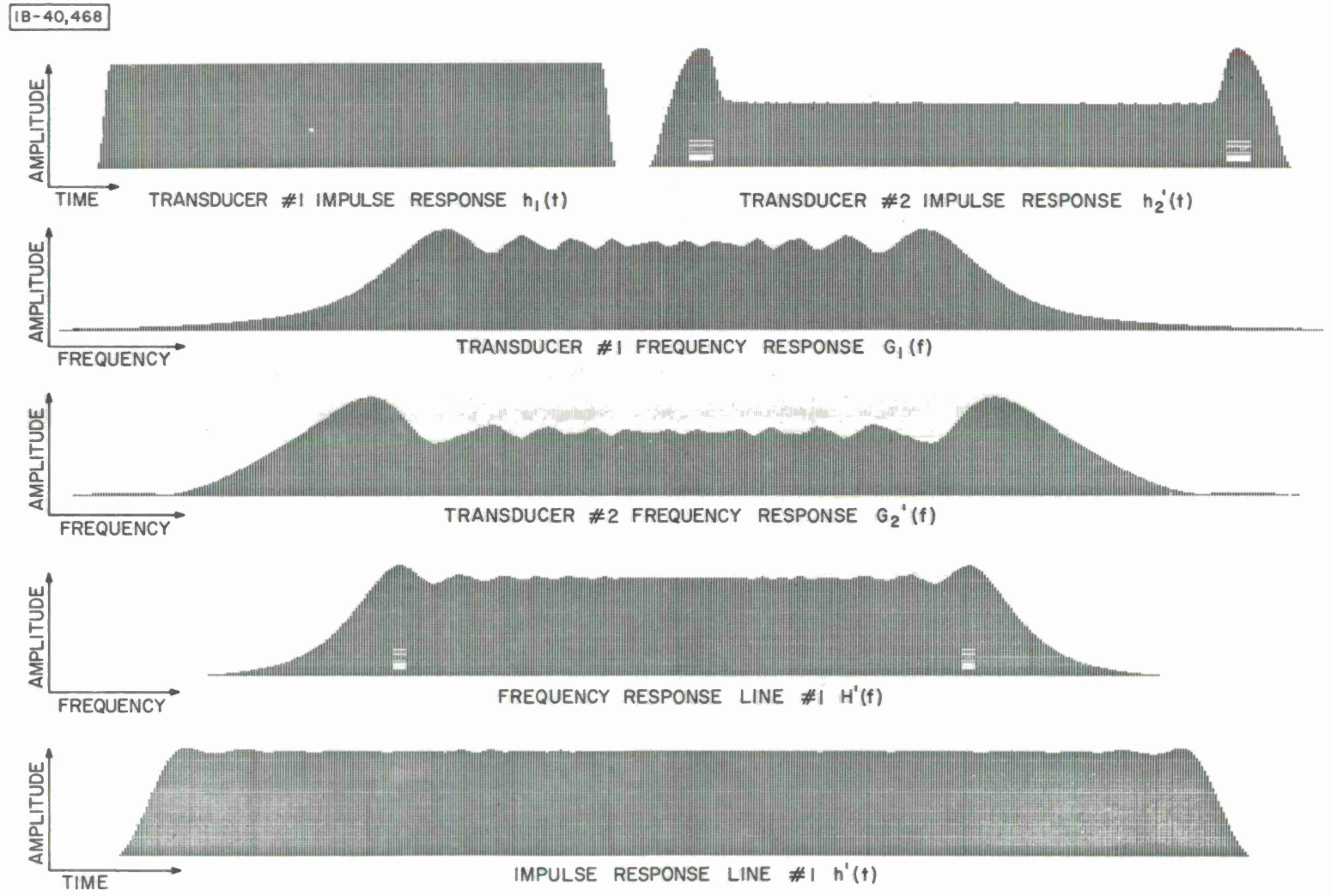

Figure 7 MITRE IMPULSE RESPONSE DESIGN

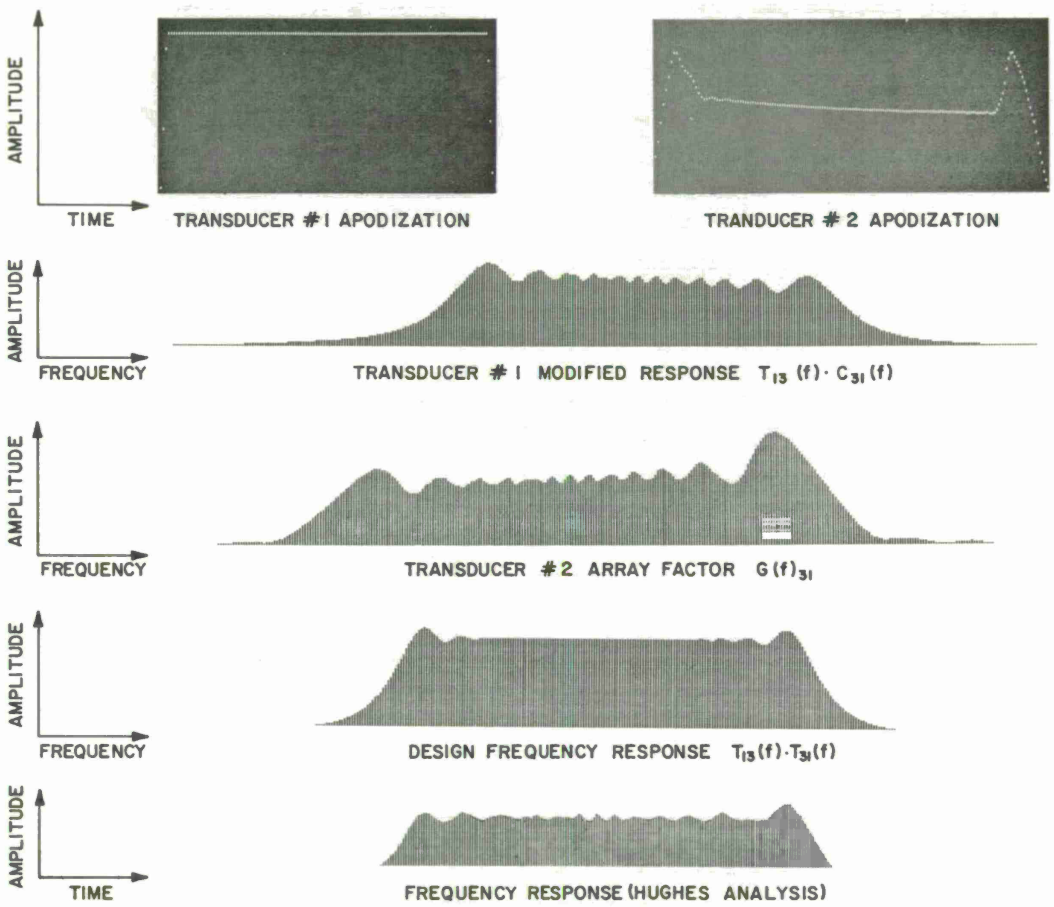

Figure 8 DISPERSIVE FILTER DESIGN

response of the entire filter. The last function represents the results obtained from the Hughes circuit analysis program for the two given transducers. This transducer analysis program predicts somewhat more ripple ($\pm$ 1/2 dB) than the waveform synthesis program. This discrepancy is currently attributed to the fact that the acoustic surface wave device is basically a tapped delay line with nonuniform tap spacing and real weighting coefficients. If this is indeed the cause, then it represents a basic limitation on the normal surface wave implementation. On the other hand, the ripple was not excessively large and it was somewhat aperiodic which would tend to spread the energy over many time sidelobes of the the compressed pulse without very serious effects. Although this discrepancy has not been completely resolved there was no obvious way to compensate for the effect in the design of the filter. Consequently the actual acoustic devices were fabricated without attempting to compensate for this effect.

The Hughes contract was for the development of seven time-contiguous dispersive filters. Each filter was to have a dispersive delay of 1.0 μsec so that the resulting impulse responses could be added contiguously after appropriate frequency translations. The details of the Hughes design were carried out for the fourth or mid-delay filter, and two master photomasks were fabricated (apodized and "unapodized"). The remaining filters were fabricated by successively stepping these master photomasks an appropriate distance to provide

the required incremental time delay. This mid-delay design was chosen to reduce the possibility of diffraction problems in any of the filters.

The theoretical and experimental results of this filter #4 design are summarized in Figures 9, 10, 11, and 12. Each figure shows the results of: 1) the MITRE waveform synthesis, 2) the Hughes circuit analysis program, and 3) the experimental measurement. Figure 9 depicts the magnitude of the frequency response or spectra. The discrepancy previously mentioned between the waveform and the circuit analysis data is evident in the first two curves. Although there is considerable randomness to the ripple structure of the measured data, many of the ripples predicted by the Hughes circuit analysis program are quite visible. This correlation provides substantiating evidence that the circuit analysis program can predict even the fine grain structure of the frequency response. The measured mid-band insertion loss is only slightly more (1.5 dB) than predicted by the analysis program and the skirt or roll-off characteristics are almost exactly as predicted.

The frequency domain quadratic phase differences are presented in Figure 10. Again the circuit analysis program predicts more phase ripple than the synthesis program, and the measured phase ripple is somewhat larger yet. However, there is again some degree of correlation between the measured and predicted phase ripples.

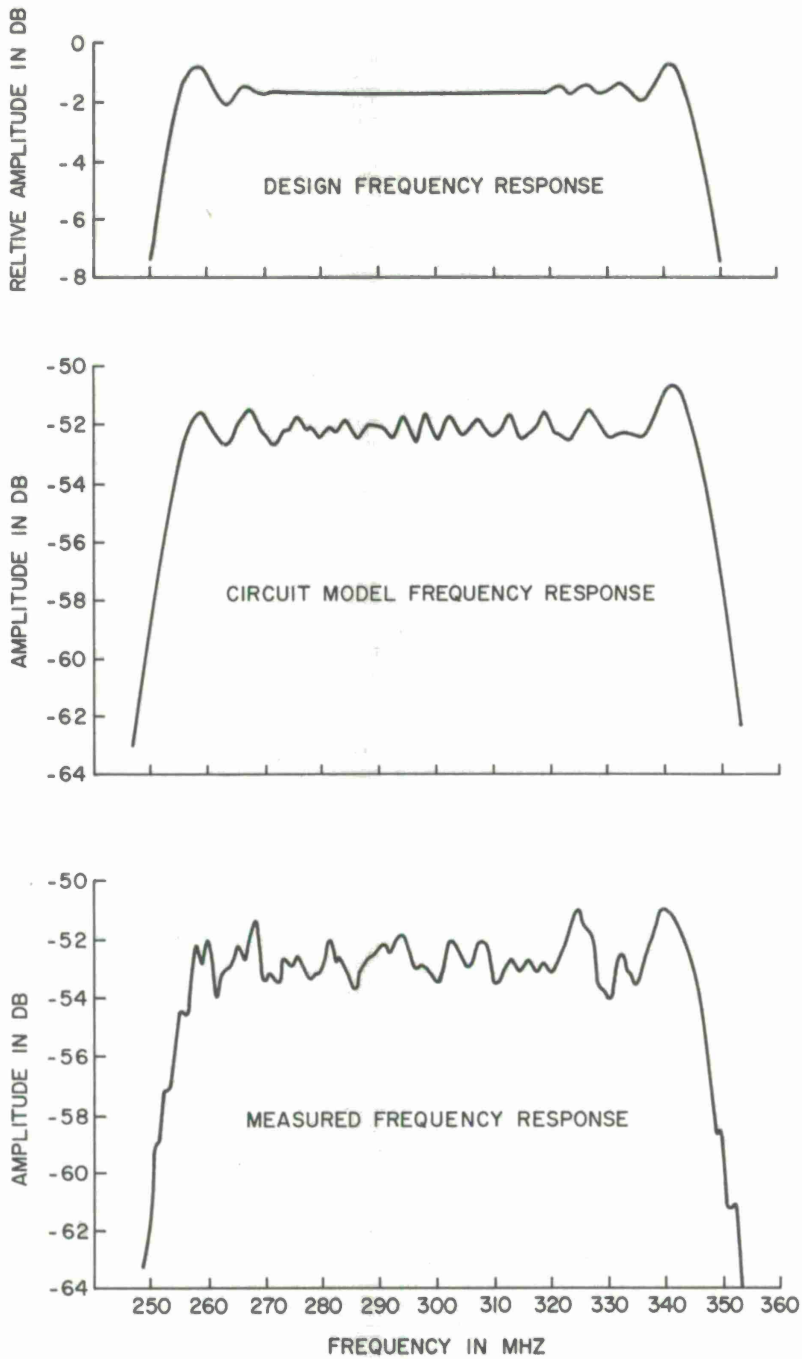

Figure 9 FREQUENCY RESPONSE

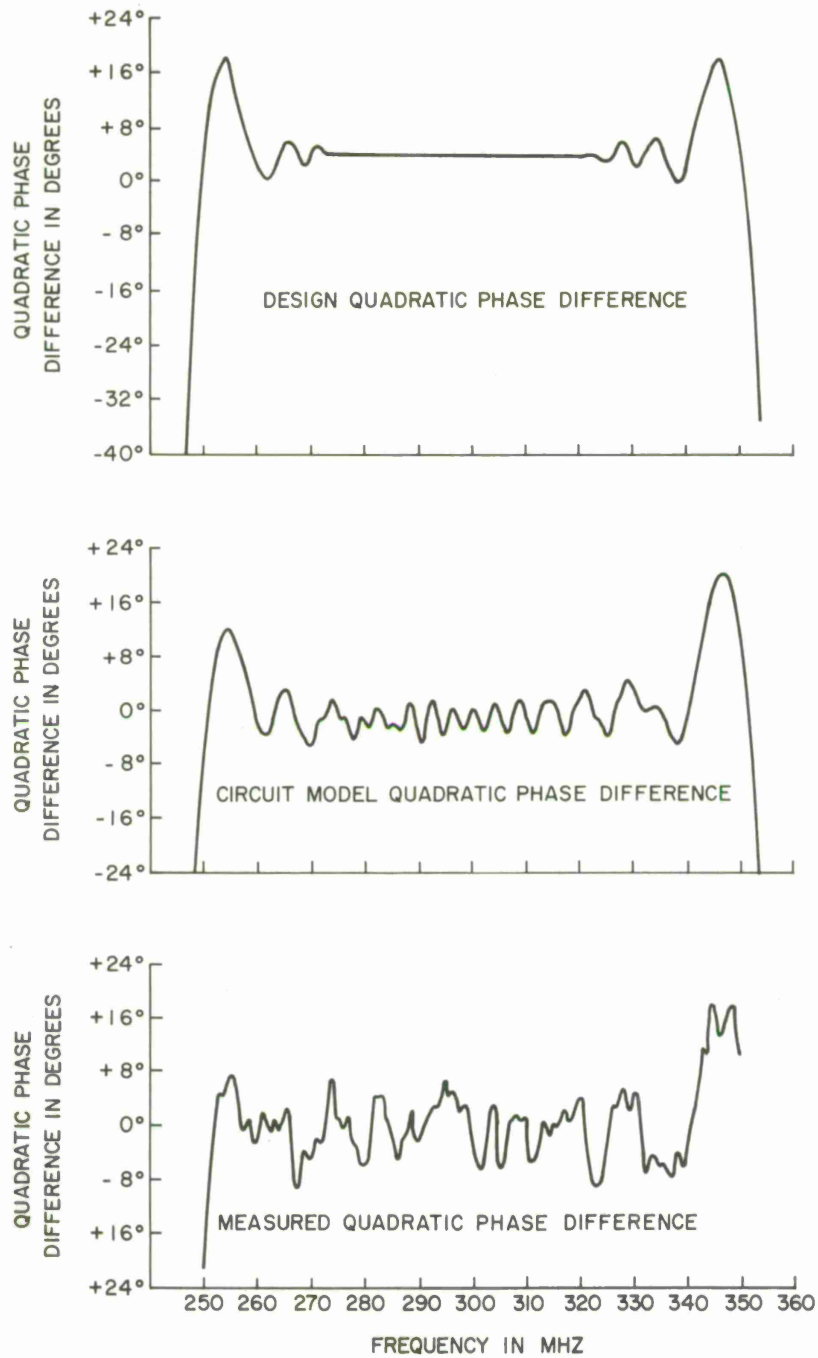

Figure 10 QUADRATIC PHASE DIFFERENCE

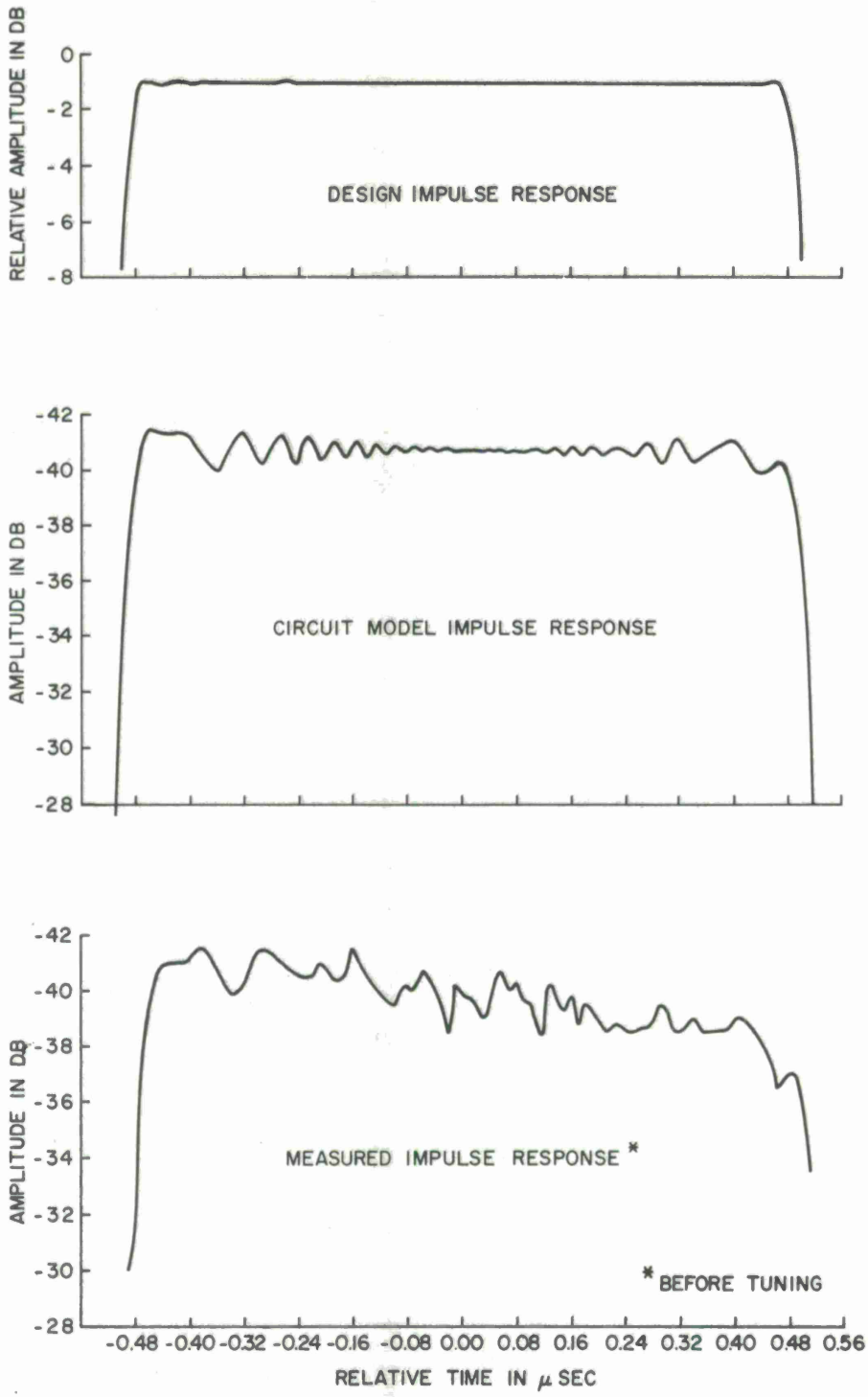

Figure 11 IMPULSE RESPONSE

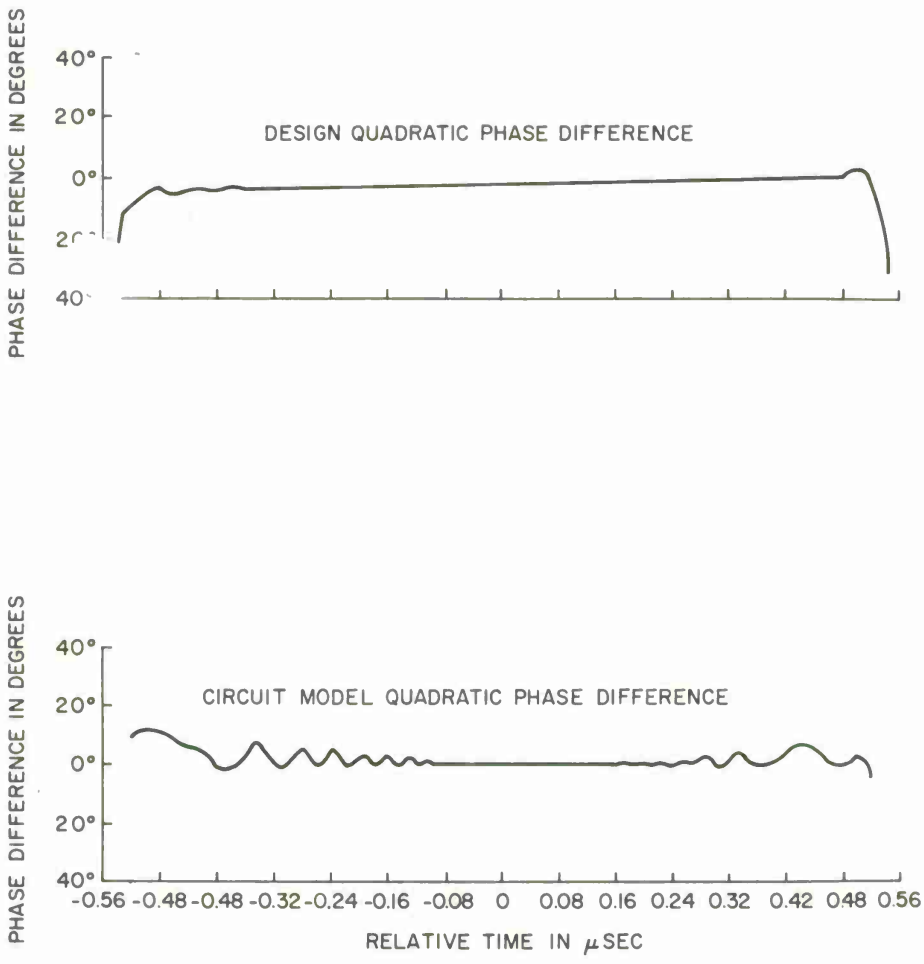

Figure 12 IMPULSE RESPONSE QUADRATIC PHASE DIFFERENCE

Figure 11 shows the analogous comparison in the time domain. There is no new data presented here as each curve is merely the Fourier transform of the analogous curves from Figures 9 and 10. The experimental data were taken using a computer controlled network analyzer with the capability of storing the information in digital form on magnetic tape. The CW frequency response data (both amplitude and phase) was taken every 200 KC from 198 MHz and 403 MHz. This experimental frequency response data was then Fourier transformed to obtain the "measured" impulse response shown as the last curve of Figure 11. It is not surprising that the extraneous ripples observed in the spectra transform to provide extraneous ripples in the impulse response. Again there is some correlation between the "measured" and predicted impulse response.

The quadratic phase difference characteristics of the filter impulse response are shown in Figure 12. The design quadratic phase difference is very nearly flat while the circuit model predicts a phase ripple on the order of $\pm 8^{\circ}$. There is no experimental data on the phase characteristics of the impulse response, but this information could be obtained from the Fourier transform of the experimental frequency response data.

The experimental frequency response data of filter #4 was also used to calculate its performance as an individual pulse compression filter. The computed recompressed pulse is shown in Figure 13. The

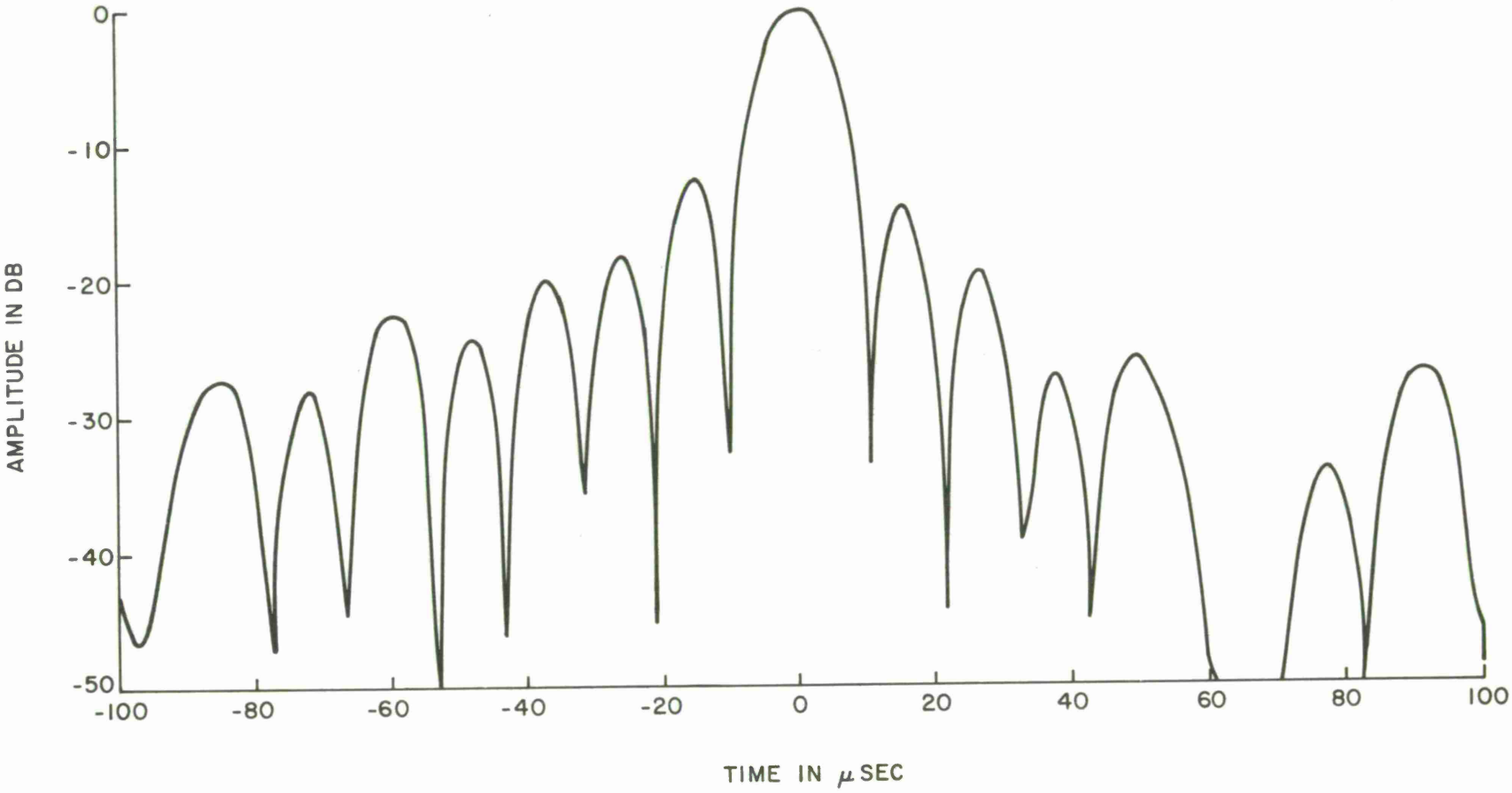

Figure 13 COMPUTED RECOMPRESSED PULSE WAVEFORM OF FILTER # 4

shape of this pulse (null-width and first side lobe level) is similar to what one would expect from an ideal linear FM impulse response with a rectangular envelope. Although the computed first side lobes are slightly non-symmetric, the average level is -14 dB as compared to a theoretical value of -13 dB; and the computed null-width is 21 Ns as compared with 20 Ns for the ideal filter. This implies that the 7% taper introduced in the design to achieve a time contiguous characteristic results in very little amplitude weighting of the response. The recompressed pulse was also measured experimentally for filter #4. This was achieved by impulsing the filter, spectrally inverting the expanded pulse, and re-applying this spectrally inverted pulse to the same filter. A photograph of this recompressed pulse is shown in Figure 14. The similarity between this and the computed result obtained from the CW measured data is striking. The non-symmetry of the first side lobes is presented in both, and their level is approximately correct. Both figures show a leading fifth side lobe which is enhanced and a trailing fifth side lobe which is suppressed. Both figures indicate an enhanced seventh side lobe, and even the relative amplitude of the leading fourth and fifth side lobe and the trailing third and fourth is similar for both figures.

The similarity of these characteristics is surprisingly exact for such diverse measurement techniques. This implies that both techniques are equally valid, and that the observed characteristics can really be attributed to the acoustic device, not the measuring

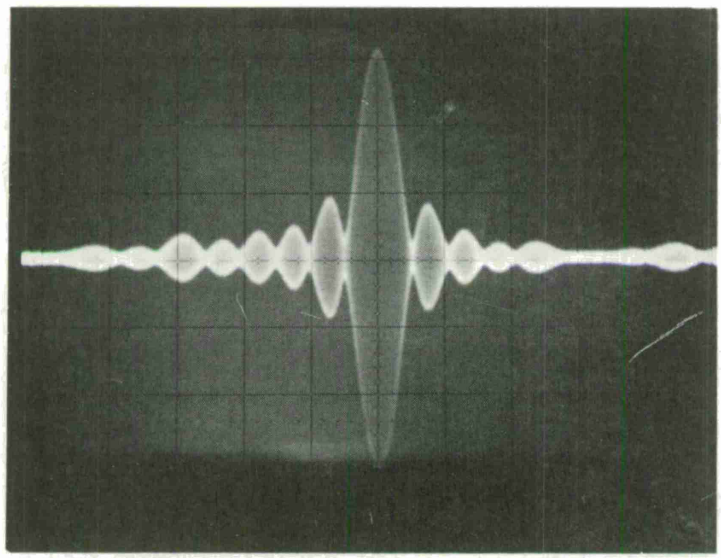

IA-43,856

Figure 14 MEASURED RECOMPRESSED PULSE OF FILTER #4

scheme. The similarity also lends credence to the idea that the entire multi-channel filter characteristics could be obtained from a computational analysis of CW frequency response data taken on each filter with the computer controlled network analyzer.

The filters built by Hughes were designed on the basis of the series tuned equivalent circuit of Figure 6 and were intended to operate with source and load resistances of 50Ω. Acoustic apertures on the order of 150 wavelengths were chosen to minimize diffraction problems, but this resulted in a radiation resistance on the order of 1/2 to 1Ω, and a total series capacitance on the order of 9 PF for the unapodized transducer and 5.6 PF for the apodized transducer. Thus in order to achieve the required input impedance match a series resistance of 50Ω was included in the filter design which resulted in a circuit factor Q_L of less than 1. This was sufficiently low that the circuit factor modification to the overall response was relatively small. On the other hand, with a radiation resistance as low as $1/2\Omega$ the circuit loss resulting from these 50Ω series resistances is about 40 dB. This series resistance is not all external. It includes parasitic loss in the tuning inductor, lead and bond resistance, and the series resistance of the thin film electrodes within the transducer. The electrode resistance of 10Ω is probably a minimum which could be practically achieved. With no

external series resistance the circuit loss would still be about 31 dB. Thus 9 dB of insertion loss is the price paid for eliminating a 5:1 mismatched input impedance. Although the Hughes design was based on a circuit Q_L which included a series resistance of 50Ω for each transducer, a compromise external resistance of 24Ω was added to keep the input impedance match better than 1.5 without introducing a full 9 dB of additional circuit loss. Even with this reduced series resistance, the change in the circuit Q_L was so small that there was no noticeable effect on the overall frequency response of the filter.

The Hughes filters were series resonated at 300 MHz with the inductance from a short length of 1 mil hook-up wire connecting the transducer summing pad to ground. For some of the unapodized transducers it was necessary to loop the wire to achieve the necessary inductance, while a second parallel wire was required to reduce the inductance for some of the apodized transducers. After tuning, the input impedance of each transducer was measured over the range of 250 MHz to 350 MHz. The resistive component of each transducer was fairly constant but did tend to gradually increase by about 10% over the frequency range. Although the reactance of each transducer was tuned out at the center frequency of 300 MHz, it did vary from -j 18Ω to +j 18Ω for the unapodized transducer and from -j 29Ω to +j 29Ω for the apodized transducer when the frequency was varied from 250 MHz

to 350 MHz. Thus the input impedance of the tuned transducer incorporating a series resistor behaved essentially as a low Q series resonant circuit.

Two identical filter #4 units were fabricated by Hughes. The first was a prototype unit which was tested extensively and the second was a final product which was packaged together with filter #5 in a single box. The measured frequency response of these two filters is shown in Figure 15. Not only are the general shapes very similar but there is considerable similarity in the fine grain ripple structure. This demonstrates the reproducibility of the characteristics and the quality of workmanship in the fabrication process.

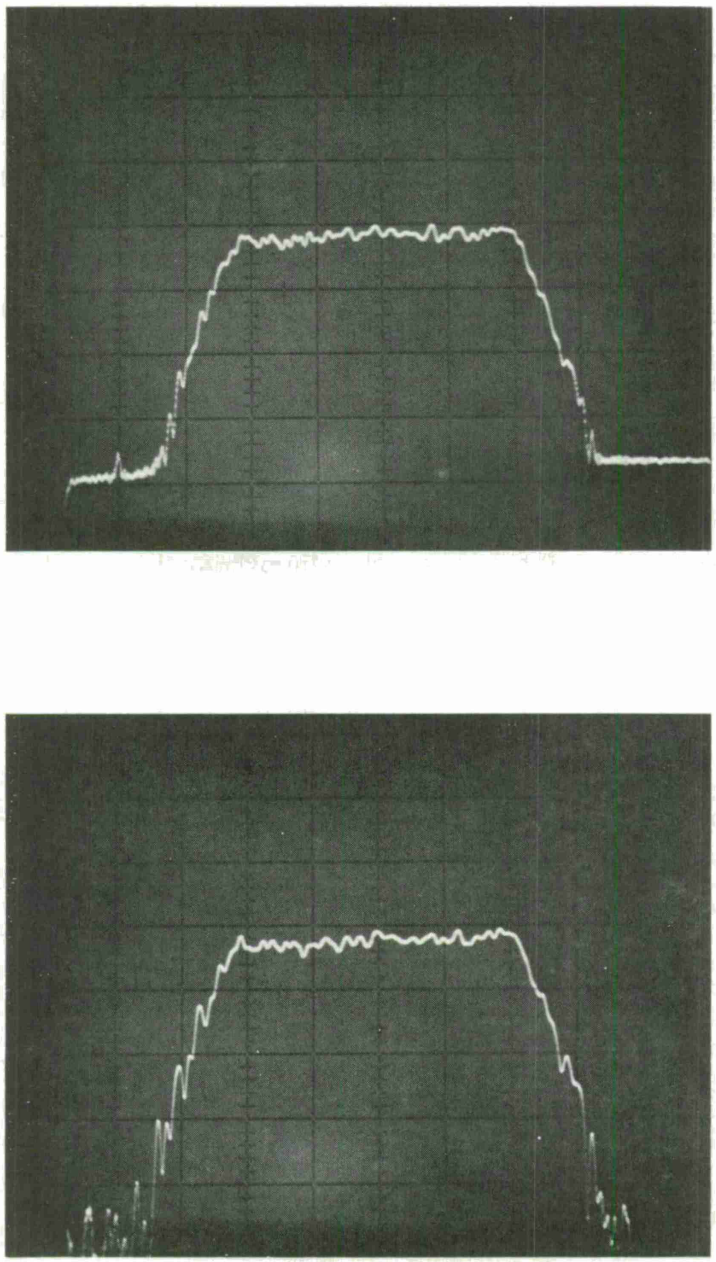

Figure 15 FREQUENCY RESPONSE OF PROTOTYPE AND FINAL FILTERS #4

SECTION 6

CONCLUSIONS AND RECOMMENDATIONS

The validity of a division synthesis technique for the realization of time-contiguous dispersive filters has been established. This technique has been used by Hughes for the design of seven acoustic surface wave filters for use in a multi-channel linear FM pulse compression system with a bandwidth capability of 700 MHz and a TW product of 4900. The resulting acoustic surface wave devices were quite reproducible and their general characteristics (spectral shape, bandwidth and dispersive delay) were essentially as desired. Although the device characteristics were well predicted by the Hughes circuit analysis program, there were slight discrepancies between the circuit analysis results and the desired waveforms. The resolution of this discrepancy should be studied although it may turn out to be a basic limitation resulting from the non-uniform electrode spacing required in a linear FM surface wave transducer.

The Hughes circuit analysis program is a powerful tool for the design of acoustic surface wave devices and it has the capability of including many second order effects. Its ability to include the effect of circuit tuning elements is of particular importance for designs such as this where the shape of the spectrum is critical.

In fact, future designs of this type should consider much lower source and load resistances such as 12.5Ω where wideband 2:1 turns ratio transformers could be employed. The use of such a transformer could reduce the midband insertion loss by 12 dB and still maintain a matched input impedance. The value of Q_L would be increased by 4 fold but the Hughes design program could readily compensate for this. The value and limitations of this technique should be investigated in any future efforts.

The technique of computing the time domain performance of a filter from measured data points in the frequency domain has been demonstrated, and it seems quite feasible to calculate the entire multi-channel filter characteristics from CW frequency response data taken on each filter with a computer controlled network analyzer. If the results of such an analysis were sufficiently promising, it would justify the additional expense to actually build the multi-channel pulse compression system.

This project has demonstrated that the technology and understanding of surface wave devices has progressed to the point where sophisticated processing schemes can be readily implemented. It should be stressed that there was no iterative cut-and-try process in the development or fabrication of these acoustic devices. These Quartz filters were designed by a division synthesis technique,

analyzed with the circuit analysis program, fabricated, tested and the major characteristics verified without the need for a redesign. This is an impressive accomplishment and both the theoreticians and experimentalists of the Hughes surface wave group deserve a great deal of credit for the achievement.

REFERENCES

1. C. E. Shannon, "Communications in the Presence of Noise," Proc. IRE, January, 1949.

2. W. R. Smith, H. M. Gerard, W. R. Jones,"Analysis and Design of Dispersive Interdigital Surface-wave Transducers" IEEE Trans. Microwave Theory Tech., Vol. MTT-20, pp 458-471, July 1972.

3. H. M. Gerard, Design of Surface Wave Filters, Lecture Notes presented at National Electronics Conference, Professional Growth Seminar, Miami Beach, Florida, December 1972.

4. W. R. Smith, Acoustic Signal Processing Devices, Semi-Annual Report, ECOM 0175-1 U.S. Army Electronics Command, Fort Monmouth, N.J., Contract DA AB07-73-C-0175, February 1974.